Linear response theory for the density matrix renormalization group: Efficient algorithms for strongly correlated excited states

Naoki Nakatani,[1,a)] Sebastian Wouters,[2] Dimitri Van Neck,[2] and Garnet Kin-Lic Chan[3,b)]
[1]*Catalysis Research Center, Hokkaido University, Kita 21 Nishi 10, Sapporo, Hokkaido 001-0021, Japan*
[2]*Center for Molecular Modeling, Ghent University, Technologiepark 903, 9052 Zwijnaarde, Belgium*
[3]*Frick Chemistry Laboratory, Department of Chemistry, Princeton University, Princeton, New Jersey 08544, USA*

(Received 7 November 2013; accepted 17 December 2013; published online 13 January 2014)

Linear response theory for the density matrix renormalization group (DMRG-LRT) was first presented in terms of the DMRG renormalization projectors [J. J. Dorando, J. Hachmann, and G. K.-L. Chan, J. Chem. Phys. **130**, 184111 (2009)]. Later, with an understanding of the manifold structure of the matrix product state (MPS) ansatz, which lies at the basis of the DMRG algorithm, a way was found to construct the linear response space for general choices of the MPS gauge in terms of the tangent space vectors [J. Haegeman, J. I. Cirac, T. J. Osborne, I. Pižorn, H. Verschelde, and F. Verstraete, Phys. Rev. Lett. **107**, 070601 (2011)]. These two developments led to the formulation of the Tamm-Dancoff and random phase approximations (TDA and RPA) for MPS. This work describes how these LRTs may be efficiently implemented through minor modifications of the DMRG sweep algorithm, at a computational cost which scales the same as the ground-state DMRG algorithm. In fact, the mixed canonical MPS form implicit to the DMRG sweep is essential for efficient implementation of the RPA, due to the structure of the second-order tangent space. We present *ab initio* DMRG-TDA results for excited states of polyenes, the water molecule, and a [2Fe-2S] iron-sulfur cluster. © *2014 AIP Publishing LLC*. [http://dx.doi.org/10.1063/1.4860375]

I. INTRODUCTION

Entanglement renormalization techniques have recently received much attention as efficient ways to solve the quantum many-body problem in lattice systems, nuclear structure, and quantum chemistry. The density matrix renormalization group (DMRG)[1,2] was the first of such techniques and is currently the most widely used. Many efficient implementations of the DMRG algorithm exist for *ab initio* quantum chemistry.[3–14] The DMRG algorithm can be understood in terms of its underlying variational ansatz, the matrix product state (MPS),[15–18] which gives a compact representation of the wavefunction on a one-dimensional lattice graph.

Although the DMRG algorithm has been very successful to investigate ground states of strongly correlated systems, there are difficulties for excited states. These arise from the fact that the optimal choice of renormalized basis states can differ for the ground and excited states. They can be renormalized separately for each state of interest, yielding an accurate but expensive result. Conversely, they can be renormalized with a single rotation matrix, which is averaged over the states of interest, yielding a less accurate but cheaper result. This issue is very similar to the one in complete active space self-consistent field (CASSCF) theory,[19] where the optimal choice of single particle orbitals can vary between the ground and excited states.

The first solution is directly targeting the state of interest with a different renormalized basis for each state. This is similar to the state-specific (SS) CASSCF algorithm. As is also the case for the SS-CASSCF algorithm, the renormalized bases of the ground and excited states are no longer orthonormal, and their overlap has to be taken into account.

In the second solution, the so-called state-averaged (SA) algorithm, a common renormalized basis is chosen for both the ground state and all excited states of interest. To compute this renormalized basis, the density matrix is averaged over all targeted states. Since the effective dimension of the renormalized basis per targeted state decreases with each extra targeted state in the SA-DMRG algorithm, it requires a larger number of renormalized basis states to achieve the same accuracy as the ground-state DMRG algorithm. One way to relieve this drawback of the SA-DMRG algorithm is to use the state-averaged harmonic Davidson (SA-HD) DMRG algorithm to target higher excited states directly.[20]

Recently, excitations have been constructed on top of a reference MPS wavefunction,[21–27] analogous to the concept of particle-hole excitations on top of a reference Slater determinant. In this post-MPS or post-DMRG theory, the reference MPS wavefunction provides a site-based mean-field ansatz,[22,28] and excitations consist of "local" changes in this mean-field ansatz.[26] In this way, analogues of the Tamm-Dancoff approximation (TDA),[24–27,29,30] the random phase approximation (RPA),[22,26,27,31] and configuration interaction with singles and doubles (CISD)[26] were derived for an MPS reference wavefunction. The main advantage of the post-DMRG theory is that it allows to derive excited state information from a ground state calculation, without the need to update or augment the renormalized basis states.

[a)]Electroni mail: naokin@cat.hokudai.ac.jp
[b)]Electronic mail: gkchan@princeton.edu

For ground-state problems, the DMRG sweep algorithm may be viewed as a particularly robust and efficient way to optimize MPS ground states. For excitations, it is therefore desirable to formulate the DMRG linear response theory (DMRG-LRT) within a similarly efficient sweep algorithm. In this work, we start from the equation of motion for a DMRG wavefunction to rederive DMRG-TDA (i.e., CI with singles) and DMRG-RPA within the DMRG language. Subsequently, we provide a step-by-step discussion of the required changes to implement these two methods in an existing DMRG code. Analysis of the computational cost shows that these methods come at the same cost as the DMRG ground-state algorithm. Finally, we compare the performance of SA-DMRG and DMRG-TDA for several excited state problems in *ab initio* quantum chemistry, to analyze the physical content of the site-based excitations in the DMRG-LRT.

II. BRIEF OVERVIEW OF THE DMRG LINEAR RESPONSE THEORY

In this section, we present a brief overview of the DMRG-LRT, derived from the time-dependent DMRG equation. This was first proposed by Dorando *et al.*[21] in the DMRG context, and later recast in the MPS language by Haegeman *et al.*,[24,25] by means of the time-dependent variational principle (TDVP).[23] Here, we follow Dorando's work in order to use the DMRG context in what follows.

A. Time-independent DMRG equation

First, we present the time-independent DMRG equation for the usual DMRG algorithm, to introduce definitions and notations. DMRG can be derived from the variational principle for an MPS wavefunction. A generic MPS wavefunction is written as

$$|\Psi\rangle = \sum_{n_1 \cdots n_k} \mathbf{A}^{n_1} \cdots \mathbf{A}^{n_i} \cdots \mathbf{A}^{n_k} |n_1 \cdots n_k\rangle , \tag{1}$$

where n_i represents the physical index, which has a dimension d, and the matrices $\mathbf{A}^{n_i}$ are of dimension $M \times M$. Due to the invariance of the matrix products, the MPS $\mathbf{A}^{n_i}$ matrices are not uniquely determined. This extra freedom is called *gauge freedom* in the MPS context. In the DMRG language, the choice of gauge is known as the *canonical form* of the DMRG wavefunction. In a DMRG sweep the matrices in the MPS wavefunction are optimized one by one. When optimizing the matrix at site i, the DMRG expresses the MPS in the mixed canonical form at that site, which can be written as

$$|\Psi\rangle = \sum_{n_1 \cdots n_k} \mathbf{L}^{n_1} \cdots \mathbf{C}^{n_i} \cdots \mathbf{R}^{n_k} |n_1 \cdots n_k\rangle . \tag{2}$$

The $\mathbf{L}^{n_i}$ and $\mathbf{R}^{n_i}$ are now called left- and right-rotation matrices, which satisfy the orthonormality conditions $\sum_{n_i} \mathbf{L}^{n_i\dagger}\mathbf{L}^{n_i} = \mathbf{1}$ and $\sum_{n_i} \mathbf{R}^{n_i}\mathbf{R}^{n_i\dagger} = \mathbf{1}$, respectively. The $\mathbf{C}^{n_i}$ is the coefficient matrix at site i, which is the current target of optimization. The DMRG wavefunction is often written in terms of renormalized states

$$|\Psi\rangle = \sum_{l_{i-1} n_i r_i} c^{n_i}_{l_{i-1} r_i} |l_{i-1} n_i r_i\rangle , \tag{3}$$

where the left- and right-renormalized bases $|l_{i-1}\rangle$ and $|r_i\rangle$ are of the form

$$|l_{i-1}\rangle = \sum_{n_1 \cdots n_{i-1}} \mathbf{L}^{n_1} \cdots \mathbf{L}^{n_{i-1}} |n_1 \cdots n_{i-1}\rangle , \tag{4}$$

$$|r_i\rangle = \sum_{n_{i+1} \cdots n_k} \mathbf{R}^{n_{i+1}} \cdots \mathbf{R}^{n_k} |n_{i+1} \cdots n_k\rangle . \tag{5}$$

Due to the orthonormality of $\mathbf{L}^{n_i}$ and $\mathbf{R}^{n_i}$, the renormalized bases also satisfy orthonormality conditions: $\langle l'_{i-1}|l_{i-1}\rangle = \delta_{l'_{i-1} l_{i-1}}$ and $\langle r'_i|r_i\rangle = \delta_{r'_i r_i}$.

In the one-site DMRG algorithm, the Lagrangian $\langle\Psi|\hat{H}|\Psi\rangle - \lambda(\langle\Psi|\Psi\rangle - 1)$ is minimized for the variations of $\mathbf{C}^{n_i}$. Consequently, the DMRG wavefunction is an eigenstate of the effective Schrödinger equation

$$\mathbf{H}_i \mathbf{C}_i = E_0 \mathbf{S}_i \mathbf{C}_i , \tag{6}$$

where the effective Hamiltonian $\mathbf{H}_i$ and the overlap matrix $\mathbf{S}_i$ are spanned by the product basis at site i, i.e., $\{\langle l'_{i-1} n'_i r'_i|\hat{H}|l_{i-1} n_i r_i\rangle\}$ and $\{\langle l'_{i-1} n'_i r'_i|l_{i-1} n_i r_i\rangle\}$, respectively, and the coefficient tensor $\mathbf{C}_i$ is a flattened view of $\{\mathbf{C}^{n_i}\}$. An important feature of the DMRG algorithm is that, because it uses the mixed-canonical form, the overlap matrix $\mathbf{S}_i$ is always the identity matrix. This leads to good numerical conditioning and is one of the reasons for the high efficiency of the DMRG algorithm. An important step of the sweep algorithm is therefore to transform the mixed-canonical form from one site to the next. In DMRG language, this is equivalent to the procedure of decimation, which ensures that we keep only M renormalized states both in the left-block $\{|l_{i-1}\rangle\}$ and the right-block $\{|r_i\rangle\}$ so that the wavefunction optimization can be performed with a polynomial complexity $\mathcal{O}(M^3k^3)$. Once $\mathbf{C}_i$ is determined from Eq. (6), the left- or right-rotation matrices can be found by means of a QR decomposition or singular value decomposition (SVD), such that

$$\mathbf{C}_i = \mathbf{L}_i \mathbf{\Lambda}_i = \mathbf{\Lambda}_{i-1} \mathbf{R}_i , \tag{7}$$

where the left- and right rotation matrices $\mathbf{L}_i$ and $\mathbf{R}_i$ are rectangular matrices having dimensions of $dM \times M$ and $M \times dM$, respectively, and $\mathbf{\Lambda}_i$ is an $M \times M$ matrix. Reshaping $\mathbf{L}_i$ to $\mathbf{L}^{n_i}$ and $\mathbf{R}_i$ to $\mathbf{R}^{n_i}$, we can then replace $\mathbf{C}^{n_i}$ by the new left (or right) rotation matrix, thereby transferring the mixed-canonical form one site to the left (or right).

B. Time-dependent DMRG equation and linear response theory

Now, we briefly introduce the time-dependent DMRG equation to derive the DMRG-LRT.[21–23,26] The time-dependent DMRG wavefunction can be written similar to Eq. (2),

$$|\Psi(t)\rangle = \sum_{n_1 \cdots n_k} \mathbf{L}^{n_1}(t) \cdots \mathbf{C}^{n_i}(t) \cdots \mathbf{R}^{n_k}(t) |n_1 \cdots n_k\rangle . \tag{8}$$

Minimizing the Dirac-Frenkel action $\langle\Psi|i\partial/\partial t - \hat{H}|\Psi\rangle$ for the variations of $\mathbf{C}^{n_i}(t)$, gives an equation of motion for the DMRG wavefunction at site i

$$i\mathbf{S}_i(t)\frac{\partial}{\partial t}\mathbf{C}_i(t) = \mathbf{H}_i(t)\mathbf{C}_i(t), \tag{9}$$

where $\mathbf{S}_i(t)$ and $\mathbf{H}_i(t)$ are the overlap and the effective Hamiltonian spanned by the product states $|l_{i-1}(t)n_i r_i(t)\rangle$ at site i. It should be noted that $\mathbf{H}_i(t)$ is always time-dependent, even if the full Hamiltonian operator $\hat{H}$ is time-independent, because the renormalized states $|l_{i-1}(t)\rangle$ and $|r_i(t)\rangle$ are time-dependent.

We can now introduce DMRG-LRT. To investigate the linear response from the time-dependent perturbation

$$\hat{V}_{\text{ext}}(t) = \hat{V}e^{-i\omega t} + \hat{V}^* e^{i\omega t}, \tag{10}$$

we introduce a perturbation expansion for the DMRG wavefunction:

$$\begin{aligned}
\mathbf{L}_i(t) &= \left(\mathbf{L}_i^{(0)} + \lambda \mathbf{L}_i^{(1)}(t) + \cdots\right)e^{-iE_0 t},\\
\mathbf{C}_i(t) &= \left(\mathbf{C}_i^{(0)} + \lambda \mathbf{C}_i^{(1)}(t) + \cdots\right)e^{-iE_0 t},\\
\mathbf{R}_i(t) &= \left(\mathbf{R}_i^{(0)} + \lambda \mathbf{R}_i^{(1)}(t) + \cdots\right)e^{-iE_0 t},
\end{aligned} \tag{11}$$

where the zeroth order elements $\mathbf{L}_i^{(0)}$, $\mathbf{C}_i^{(0)}$, and $\mathbf{R}_i^{(0)}$ are determined by the time-independent DMRG equation, Eq. (6), and are from now on fixed for each site i. We next insert Eq. (11) in Eq. (9), and collect the first order terms per Fourier mode. This gives a pair of frequency-dependent DMRG linear response equations for each site i

$$\left(\mathbf{H}_i^{(0)} - (E_0 - \omega)\mathbf{1}\right)\mathbf{C}_{i,+\omega}^{(1)} = -\mathbf{Q}_i^C\left(\Delta\mathbf{H}_{i,+\omega}^{(1)} + \mathbf{V}_i^{(1)}\right)\mathbf{C}_i^{(0)}, \tag{12}$$

$$\left(\mathbf{H}_i^{(0)} - (E_0 + \omega)\mathbf{1}\right)\mathbf{C}_{i,-\omega}^{(1)} = -\mathbf{Q}_i^C\left(\Delta\mathbf{H}_{i,-\omega}^{(1)} + \mathbf{V}_i^{(1)*}\right)\mathbf{C}_i^{(0)}, \tag{13}$$

where $\mathbf{Q}_i^C = \mathbf{1} - \mathbf{C}_i^{(0)}\mathbf{C}_i^{(0)^\dagger}$ and $\Delta\mathbf{H}_{i,\pm\omega}^{(1)}$ is the first order change of the effective Hamiltonian at site i.

The first order DMRG wavefunction is of the explicit form

$$\begin{aligned}
|\Psi_{\pm\omega}^{(1)}\rangle = \sum_{n_1\cdots n_k} \big[&\mathbf{L}_{\pm\omega}^{n_1(1)}\cdots\mathbf{C}^{n_i(0)}\cdots\mathbf{R}^{n_k(0)} + \cdots\\
&+\mathbf{L}^{n_1(0)}\cdots\mathbf{C}_{\pm\omega}^{n_i(1)}\cdots\mathbf{R}^{n_k(0)} + \cdots\\
&+\mathbf{L}^{n_1(0)}\cdots\mathbf{C}^{n_i(0)}\cdots\mathbf{R}_{\pm\omega}^{n_k(1)}\big]\,|n_1\cdots n_k\rangle\,,
\end{aligned} \tag{14}$$

where the $+\omega$ and $-\omega$ components correspond to the forward and backward propagating parts in time, respectively. It is well known that in linear response theory, no loss of variational freedom occurs by restricting $|\Psi^{(0)}\rangle \perp |\Psi^{(1)}\rangle$. The projector $\mathbf{Q}_i^C$ in Eqs. (12) and (13) ensures that $\mathbf{C}_{i,\pm\omega}^{(1)\ \dagger}\cdot\mathbf{C}_i^{(0)} = 0$. In addition, further conditions must also be placed on the first order changes in the left- and right-rotation matrices. In previous work,[21] it was shown that these conditions are

$$\sum_{n_k}\mathbf{L}^{n_k(1)^\dagger}\mathbf{L}^{n_k(0)} = \mathbf{0}, \tag{15}$$

to the left of the current site (site i in Eq. (14)) and

$$\sum_{n_k}\mathbf{R}^{n_k(0)}\mathbf{R}^{n_k(1)^\dagger} = \mathbf{0}, \tag{16}$$

to the right of this site. As is further shown in Refs. 23 and 26, all gauge freedom in the first order wavefunction is fixed this way.

An efficient solution of the linear response (LR) equations (12), (13) is achieved by solving them at each site in a DMRG sweep. As discussed in Sec. II A, this requires shifting the mixed canonical form from one site to the next. In Ref. 21, this was achieved by writing down the linear response equations for the left and right rotation matrices in terms of the first order density matrices. For the left rotation matrix, the response equation is of the form

$$\left(\mathbf{D}_L^{(0)} - \sigma_p\mathbf{1}\right)\mathbf{l}_p^{(1)} = -\mathbf{Q}_i^L\mathbf{D}_L^{(1)}\mathbf{l}_p^{(0)}, \tag{17}$$

where the zeroth and the first order density matrices, $\mathbf{D}_L^{(0)}$ and $\mathbf{D}_L^{(1)}$ are given by

$$\begin{aligned}
\mathbf{D}_L^{(0)} &= \mathrm{Tr}_R\left[\mathbf{C}_i^{(0)}\mathbf{C}_i^{(0)^\dagger}\right],\\
\mathbf{D}_L^{(1)} &= \mathrm{Tr}_R\left[\mathbf{C}_i^{(1)}\mathbf{C}_i^{(0)^\dagger}\right] + h.c.
\end{aligned} \tag{18}$$

$\mathbf{l}_p^{(0)}$ and $\mathbf{l}_p^{(1)}$ are the pth renormalized basis states in the zeroth and the first order spaces, respectively, σ_p is the pth eigenvalue of $\mathbf{D}_L^{(0)}$, and the projector $\mathbf{Q}_i^L$ is defined as

$$\mathbf{Q}_i^L = \mathbf{1} - \sum_p^M \mathbf{l}_p^{(0)}\mathbf{l}_p^{(0)^\dagger} = \mathbf{1} - \mathbf{L}_i^{(0)}\mathbf{L}_i^{(0)^\dagger}. \tag{19}$$

To solve (17), we get the first order left rotation matrix as $\mathbf{L}_i^{(1)} = \{\mathbf{l}_p^{(1)}\}_{1\le p\le M}$.

Here, we formulate the transformation in terms of the coefficient matrices directly. In the zeroth order wavefunction, the mixed-canonical form is shifted between sites with Eq. (7):

$$\mathbf{C}_i^{(0)}\mathbf{R}_{i+1}^{(0)} = \mathbf{L}_i^{(0)}\mathbf{\Lambda}_i\mathbf{R}_{i+1}^{(0)} = \mathbf{L}_i^{(0)}\mathbf{C}_{i+1}^{(0)}, \tag{20}$$

where the left factors of each term are $dM \times M$ matrices, the right factors are $M \times dM$ matrices, and $\mathbf{\Lambda}_i$ is the $M \times M$ matrix describing the choice of the gauge at the ith boundary:

$$\mathbf{\Lambda}_i = \mathbf{L}_i^{(0)^\dagger}\mathbf{C}_i^{(0)} = \mathbf{C}_{i+1}^{(0)}\mathbf{R}_{i+1}^{(0)\ \dagger}. \tag{21}$$

To shift the mixed canonical form in the first order part of the wavefunction, consider all first order contributions on the relevant sites. The transformation we would like to achieve is

$$\mathbf{C}_i^{(1)}\mathbf{R}_{i+1}^{(0)} + \mathbf{C}_i^{(0)}\mathbf{R}_{i+1}^{(1)} = \mathbf{L}_i^{(1)}\mathbf{C}_{i+1}^{(0)} + \mathbf{L}_i^{(0)}\mathbf{C}_{i+1}^{(1)}. \tag{22}$$

Given the left (right) part, can we find a solution for the right (left) part of the equation? We start with the right-to-left case. Multiplying Eq. (22) with $\mathbf{R}_{i+1}^{(0)\ \dagger}$ to the right gives

$$\mathbf{C}_i^{(1)} = \mathbf{L}_i^{(1)}\mathbf{C}_{i+1}^{(0)}\mathbf{R}_{i+1}^{(0)\ \dagger} + \mathbf{L}_i^{(0)}\mathbf{C}_{i+1}^{(1)}\mathbf{R}_{i+1}^{(0)\ \dagger}. \tag{23}$$

Multiplying Eq. (22) with $\mathbf{Q}_{i+1}^R = \mathbf{1} - \mathbf{R}_{i+1}^{(0)\ \dagger}\mathbf{R}_{i+1}^{(0)}$ to the right and $\mathbf{\Lambda}_i^{-1}\mathbf{L}_i^{(0)^\dagger}$ to the left gives

$$\mathbf{R}_{i+1}^{(1)} = \mathbf{\Lambda}_i^{-1}\mathbf{C}_{i+1}^{(1)}\mathbf{Q}_{i+1}^R. \tag{24}$$

The first order terms on the LHS of Eq. (22) can hence be calculated if the RHS is known. Analogously, the left-to-right case yields the equations

$$\mathbf{C}_{i+1}^{(1)} = \mathbf{L}_i^{(0)^\dagger}\mathbf{C}_i^{(1)}\mathbf{R}_{i+1}^{(0)} + \mathbf{L}_i^{(0)^\dagger}\mathbf{C}_i^{(0)}\mathbf{R}_{i+1}^{(1)}, \tag{25}$$

$$\mathbf{L}_i^{(1)} = \mathbf{Q}_i^L\mathbf{C}_i^{(1)}\mathbf{\Lambda}_i^{-1}, \tag{26}$$

with $\mathbf{Q}_i^L = \mathbf{1} - \mathbf{L}_i^{(0)}\mathbf{L}_i^{(0)\dagger}$. These relations enable to change the canonical form of the first order wavefunction to perform an efficient sweep algorithm for DMRG-LRT. Note that Eqs. (23) and (25) are very similar to the guess wavefunction transformation of the one-site DMRG algorithm.[5] The left and right projectors $\mathbf{Q}_i^L$ and $\mathbf{Q}_i^R$ hold the first order rotation matrices to be orthogonal to the zeroth order contributions, so that they satisfy Eqs. (15) and (16), respectively.

C. Tamm-Dancoff approximation and random phase approximation

The LR equations define a first order wavefunction which determines the dynamic response of observables, such as spectral functions. From the poles of the response, we obtain excited states and their eigenvalues. Formulating the determination of the poles as an eigenvalue problem yields the Tamm-Dancoff and random phase approximations to excited states in DMRG. An explicit route to derive the DMRG-TDA and DMRG-RPA eigenvalue equations is to use a linearization of the time-dependent variational principle,[22,26,27] from which the TDA can be understood as a variational approximation to RPA. Our objective here is to formulate an efficient sweep algorithm to solve the DMRG-TDA and DMRG-RPA equations. To do so, we first recall the DMRG-RPA eigenvalue problem

$$\begin{pmatrix} \mathbf{H} & \mathbf{W} \\ \mathbf{W}^* & \mathbf{H}^* \end{pmatrix} \begin{pmatrix} \mathbf{X} \\ \mathbf{Y} \end{pmatrix} = \omega \begin{pmatrix} \mathbf{S} & \mathbf{0} \\ \mathbf{0} & -\mathbf{S}^* \end{pmatrix} \begin{pmatrix} \mathbf{X} \\ \mathbf{Y} \end{pmatrix}, \tag{27}$$

where $\mathbf{H}$, $\mathbf{W}$, and $\mathbf{S}$ are $dM^2k \times dM^2k$ matrices. Their $dM^2 \times dM^2$ block components (depending on the site indices i and j) are

$$\mathbf{H}_{ij} = \langle \partial_i \Psi^{(0)} | \hat{H} - E_0 | \partial_j \Psi^{(0)} \rangle , \tag{28}$$

$$\mathbf{W}_{ij} = \langle \partial_i \partial_j \Psi^{(0)} | \hat{H} - E_0 | \Psi^{(0)} \rangle , \tag{29}$$

$$\mathbf{S}_{ij} = \langle \partial_i \Psi^{(0)} | \partial_j \Psi^{(0)} \rangle , \tag{30}$$

where $|\partial_i \Psi^{(0)}\rangle$ and $|\partial_i \partial_j \Psi^{(0)}\rangle$ are the first and second order derivatives of the DMRG wavefunction with respect to the site components $\mathbf{A}_i$

$$|\partial_i \Psi^{(0)}\rangle = \hat{Q}_i^{(1)} \frac{\partial}{\partial \mathbf{A}_i} |\Psi^{(0)}\rangle , \tag{31}$$

$$|\partial_i \partial_j \Psi^{(0)}\rangle = \hat{Q}_{ij}^{(2)} \frac{\partial^2}{\partial \mathbf{A}_i \partial \mathbf{A}_j} |\Psi^{(0)}\rangle . \tag{32}$$

The site components $\mathbf{A}_i$ can be in one of the canonical forms $\{\mathbf{L}_i^{(0)}, \mathbf{C}_i^{(0)}, \mathbf{R}_i^{(0)}\}$, depending on the canonical form of $|\Psi^{(0)}\rangle$. The operator $\hat{Q}^{(n)}$ projects the bare derivative to the nth order subspace orthogonal to all lower order subspaces, as discussed later. The dM^2k dimensional vectors $\mathbf{X} = \{\boldsymbol{x}_1, \cdots, \boldsymbol{x}_k\}$ and $\mathbf{Y} = \{\boldsymbol{y}_1, \cdots, \boldsymbol{y}_k\}$ in Eq. (27) represent the forward and backward propagating RPA amplitudes.

If $|\Psi^{(0)}\rangle$ is accurate enough, the $\mathbf{W}$ matrix vanishes because $(\hat{H} - \hat{E}_0)|\Psi^{(0)}\rangle \approx 0$, which leads to the Tamm-Dancoff approximation

$$\mathbf{HX} = \omega \mathbf{SX}, \tag{33}$$

which is a variational method which targets excitations in the subspace spanned by $\{|\partial_i \Psi^{(0)}\rangle\}$.

D. Non-redundant parameterizations of the first and second order spaces

The space spanned by the bare derivatives contains lower order derivatives. The first order space $\{\partial/\partial \mathbf{A}_i |\Psi^{(0)}\rangle\}$ contains, for example, $|\Psi^{(0)}\rangle$, and the second order space $\{\partial^2/\partial \mathbf{A}_i \partial \mathbf{A}_j |\Psi^{(0)}\rangle\}$ contains both $\{|\partial_i \Psi^{(0)}\rangle\}$ and $|\Psi^{(0)}\rangle$. In LRT, we look for independent changes orthogonal to the reference wavefunction, and therefore want to express derivative subspaces which are orthogonal to lower order derivative subspaces. In this study, we focus on a so-called non-redundant parameterization in terms of the projectors $\hat{Q}^{(n)}$, while previous studies focused on explicit expressions for the tangent space vectors in MPS terminology.[23,26,27]

The projectors for the first order space were already introduced during the discussion of DMRG-LRT in Eqs. (12)–(26), i.e., the representation of $\hat{Q}_i^{(1)}$ is chosen from $\{\mathbf{Q}_i^C, \mathbf{Q}_i^L, \mathbf{Q}_i^R\}$, depending on the choice of the canonical form at site i. The mixed-canonical form of Eq. (2) then results in an overlap matrix $\mathbf{S}_{ij}$ which is block diagonal in the site-indices. A diagonal block $\mathbf{S}_{ii}$ is of the form

$$\mathbf{S}_{ii} = \mathbf{Q}_i^{(1)\dagger} \mathbf{Q}_i^{(1)}, \tag{34}$$

where it should be noted that the rank of the $dM^2 \times dM^2$ matrix $\mathbf{S}_{ii}$ is now only $(d-1)M^2$, equal to the number of non-redundant parameters at site i, because $\mathbf{Q}_i^{(1)}$ explicitly projects out the zeroth order contributions.

The MPS tangent space vectors are normalized basis vectors in the span of $\mathbf{Q}_i^{(1)}$. The connection between the projector and non-redundant tangent space parameterization of the MPS is discussed in detail in Ref. 26. Briefly, an explicit parameterization of the non-redundant tangent space vectors is given by

$$\mathcal{T}_{\mathbf{A}} |\Psi^{(0)}\rangle = \frac{1}{k} \sum_i \mathbf{B}_i \frac{\partial}{\partial \mathbf{A}_i} |\Psi^{(0)}\rangle , \tag{35}$$

where $\mathbf{B}_i$ describes the null-space projection $\{l_{i-1}\} \times \{n_i\} \to \{l_i\}^{\perp}$ which is given by the $dM \times (d-1)M$ matrix satisfying $\mathbf{B}_i^\dagger \mathbf{B}_i = \mathbf{1}$ and $\mathbf{B}_i^\dagger \mathbf{A}_i^{(0)} = \mathbf{0}$ for the left-fixed gauge condition. The first order change is then parameterized by the $(d-1)M \times M$ matrix $\boldsymbol{x}_i$, which is related to the projector formalism by

$$\mathbf{L}_i^{(1)} = \mathbf{B}_i \boldsymbol{x}_i \boldsymbol{\Lambda}_i^{-1}. \tag{36}$$

For the second order derivative, the projector $\hat{Q}_{ij}^{(2)}$ cannot be simply defined for any gauge choice. However, in the mixed-canonical form, we can define the second order projector as the product of first order projectors, $\hat{Q}_{ij}^{(2)} = \hat{Q}_i^{(1)} \times \hat{Q}_j^{(1)}$. To check this, we investigate whether the overlap $\langle \partial_i \partial_j \Psi^{(0)} | \partial_p \Psi^{(0)} \rangle$ is zero or not in this gauge.

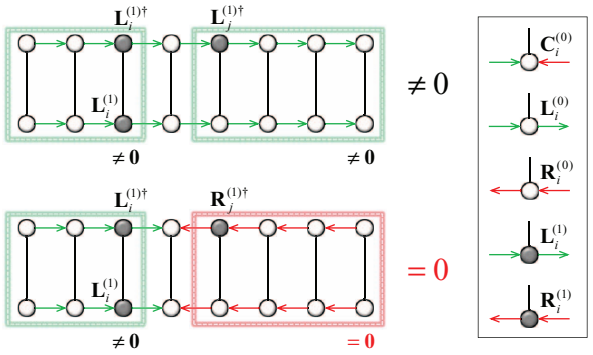

FIG. 1. Non-redundant parameterization for the second order derivative. The top panel shows the redundancy between the first and second derivatives with the left-canonical gauge. The bottom panel shows the non-redundant parameterization with the mixed-canonical gauge in between sites i and j.

If the site index of p is different from the site indices of i and j, the overlap is zero (in fact, for any gauge choice) since at least one of the first order projectors gives null. The non-trivial case occurs when the site corresponding to p also corresponds to either i or j. Consider p and i to be on the same site within the mixed-canonical gauge, if $\mathbf{C}_q^{(0)}$ is in between sites i and j, the overlap is zero because of the orthogonality in the right block, $\sum_{n_j} \mathbf{R}^{n_j(0)}\mathbf{R}^{n_j(1)\dagger} = \mathbf{0}$ (see Fig. 1). Consequently, the non-redundant parameterization of the second order space is achieved in a simple manner within the mixed-canonical form employed with the DMRG sweep. (Note, however, that for the third and higher order spaces, it seems to be impossible to simply define the projector $\hat{Q}^{(n)}$ as a product of the lower order projectors, e.g., $\hat{Q}^{(3)}_{ijk} = \hat{Q}^{(1)}_i \times \hat{Q}^{(1)}_j \times \hat{Q}^{(1)}_k$.)

III. DAVIDSON ALGORITHM FOR DMRG-TDA AND DMRG-RPA

We now present an efficient algorithm that will allow us to solve the DMRG-TDA and DMRG-RPA eigenvalue problems within the context of a DMRG sweep. The eigenvectors in the DMRG-TDA and DMRG-RPA are typically large, with $\mathcal{O}(dM^2k)$ elements. As we are usually interested in only a few excited states, the iterative Davidson algorithm is ideal for this purpose[32] (Note that unlike in the ground-state DMRG, the Davidson algorithm is working here in the space of first order wavefunctions, i.e., the solutions are linear combinations of MPS). The basic idea is to formulate all the operations in the Davidson algorithm, such as the matrix-vector multiplication, in terms of a DMRG sweep. Initially, we focus on DMRG-TDA to explain our basic algorithm, and later we explain its generalization for DMRG-RPA.

A. Overall structure of the DMRG-TDA computations

In the Davidson algorithm, a full matrix representation is projected into a small matrix spanned by a small number of trial vectors. In the case that several eigenvalues are desired, the block-variant of the Davidson algorithm is commonly used. Its pseudocode is shown in Fig. 2.

For DMRG-TDA, one particular choice $\mathbf{X} = \{\mathbf{L}_1^{(1)}, \cdots, \mathbf{C}_i^{(1)}, \cdots, \mathbf{R}_k^{(1)}\}$ of first order changes in the DMRG

choose n trial vectors $\mathbf{V}_1 = \{\boldsymbol{x}_1, \ldots, \boldsymbol{x}_n\}$
for $i = 1, 2, \ldots$ **do**
  $m \leftarrow \dim(\mathbf{V}_i)$
  $\mathbf{W}_i^H \leftarrow \mathbf{H}\mathbf{V}_i$, $\mathbf{H}_R \leftarrow \mathbf{V}_i^\dagger \mathbf{W}_i^H$
  $\mathbf{W}_i^S \leftarrow \mathbf{S}\mathbf{V}_i$, $\mathbf{S}_R \leftarrow \mathbf{V}_i^\dagger \mathbf{W}_i^S$
  solve m eigenpairs $\{\omega_\mu, \boldsymbol{\alpha}_\mu\}$ of $\mathbf{H}_R\boldsymbol{\alpha}_\mu = \omega_\mu \mathbf{S}_R\boldsymbol{\alpha}_\mu$
  for $\mu = 1 \to m$ **do**
    $\mathbf{u}_\mu \leftarrow \mathbf{V}_i\boldsymbol{\alpha}_\mu$
    $\mathbf{p}_\mu \leftarrow \mathbf{W}_i^H\boldsymbol{\alpha}_\mu$, $\mathbf{q}_\mu \leftarrow \mathbf{W}_i^S\boldsymbol{\alpha}_\mu$
    $\mathbf{r}_\mu \leftarrow \mathbf{p}_\mu - \omega_\mu\mathbf{q}_\mu$
  end for
  if $\{|\boldsymbol{r}_\mu|^2 < \epsilon : 1 \le \mu \le n\}$ **then**
    Exit on Convergence
  end if
  for $\mu = 1 \to n$ **do**
    $\mathbf{z}_\mu \leftarrow -(\mathbf{H} - \omega_\mu\mathbf{S})^{-1}\mathbf{r}_\mu$
  end for
  if $m \le N - n$ **then**
    $\mathbf{V}_{i+1} \leftarrow \{\mathbf{u}_1, \ldots, \mathbf{u}_m, \mathbf{z}_1, \ldots, \mathbf{z}_n\}$
  else
    $\mathbf{V}_{i+1} \leftarrow \{\mathbf{u}_1, \ldots, \mathbf{u}_n, \mathbf{z}_1, \ldots, \mathbf{z}_n\}$ ▷ Deflation
  end if
end for

FIG. 2. Pseudocode of the block-Davidson algorithm for generalized eigenvalue problems (GEP), where n is the number of desired roots, ϵ is a certain (small) threshold, and N is the maximum number of trial vectors. Upon convergence, $\{\omega_\mu, \mathbf{u}_\mu : 1 \le \mu \le n\}$ are the eigenvalues and eigenvectors, respectively.

wavefunction is a trial vector, which has a dimension of dM^2k. This trial vector represents formally a linear combination of MPS, of the form in Eq. (14).

Important for an efficient implementation of DMRG-TDA (and DMRG-RPA) is how to efficiently compute (1) the projected matrices $\mathbf{H}_R$ and $\mathbf{S}_R$, where the subscript R means "reduced" matrix in the small subspace, (2) the eigenvectors as a rotation of the basis vectors by the Ritz vectors $\boldsymbol{\alpha}$, and (3) the correction vectors $\mathbf{z}$, because they involve matrix/vector multiplications which have the large linear dimension dM^2k. A naive implementation of the matrix-vector multiplications would cost $\mathcal{O}(M^4)$. Fortunately, they can be carried out with at most $\mathcal{O}(M^3)$ complexity by means of the sweep algorithm, as discussed in Secs. III B–III E.

B. Sweep algorithm for the projected Hamiltonian

Suppose we have m trial vectors for the first order wavefunctions in the left-canonical form, i.e., $\mathbf{X}_\mu = \{\mathbf{L}_1^{\mu(1)}, \cdots, \mathbf{L}_k^{\mu(1)}\}_{1\le\mu\le m}$. The matrix elements of the projected Hamiltonian $\mathbf{H}_R$ are then given by

$$H_{\mu\nu} = \left\langle \Psi_\mu^{(1)} \middle| \hat{H} \middle| \Psi_\nu^{(1)} \right\rangle = \sum_{ij} \mathbf{L}_i^{\mu(1)\dagger} \mathbf{H}_{ij} \mathbf{L}_j^{\nu(1)}. \tag{37}$$

To construct a sweep algorithm, it is necessary to break up the overall matrix/vector computation into site-by-site computations, such that

$$H_{\mu\nu} = \sum_{i=1}^{k} H_{\mu\nu}^{[i]}, \tag{38}$$

where $H^{[i]}_{\mu\nu}$ is defined as a (left-) block component at site i

$$H^{[i]}_{\mu\nu} = \mathbf{L}_i^{\mu(1)\dagger}\mathbf{H}^{(0)}_{ii}\mathbf{L}_i^{\nu(1)} + \sum_{j=1}^{i-1}\left(\mathbf{L}_i^{\mu(1)\dagger}\mathbf{H}^{(0)}_{ij}\mathbf{L}_j^{\nu(1)} + \mathbf{L}_j^{\mu(1)\dagger}\mathbf{H}^{(0)}_{ji}\mathbf{L}_i^{\nu(1)}\right). \quad (39)$$

Taking the summation over j and using the first order gauge condition in Eq. (22), we get

$$H^{[i]}_{\mu\nu} = \tilde{\mathbf{C}}_i^{\mu(1)\dagger}\mathbf{H}_0^{[i]}\tilde{\mathbf{C}}_i^{\nu(1)} + \tilde{\mathbf{C}}_i^{\mu(1)\dagger}\Delta\mathbf{H}_\nu^{[i]}\mathbf{C}_i^{(0)} + \mathbf{C}_i^{(0)\dagger}\Delta\mathbf{H}_\mu^{[i]\dagger}\tilde{\mathbf{C}}_i^{\nu(1)}, \quad (40)$$

where $\mathbf{H}_0^{[i]}$ and $\Delta\mathbf{H}_\mu^{[i]}$ are the zeroth and first order *superblock* operators, respectively, in the left-block component

$$\mathbf{H}_0^{[i]} = \mathbf{H}_0^{L_{i-1}} \times \mathbf{h}_i \times \mathbf{H}_0^{R_i}, \quad (41)$$

$$\Delta\mathbf{H}_\mu^{[i]} = \mathbf{H}_\mu^{L_{i-1}} \times \mathbf{h}_i \times \mathbf{H}_0^{R_i}. \quad (42)$$

In this equation, $\mathbf{h}_i$ contains the local operators acting on site i. $\mathbf{H}_0^{L_{i-1}}$ and $\mathbf{H}_0^{R_i}$ are the zeroth order left- and right-renormalized operators, respectively. $\mathbf{H}_\mu^{L_{i-1}}$ is the first order left-renormalized operator given by

$$\mathbf{H}_\mu^{L_{i-1}} = \mathbf{L}_{i-1}^{(0)\dagger}\left[\mathbf{H}_\mu^{L_{i-2}} \times \mathbf{h}_{i-1}\right]\mathbf{L}_{i-1}^{(0)} + \mathbf{L}_{i-1}^{(0)\dagger}\left[\mathbf{H}_0^{L_{i-2}} \times \mathbf{h}_{i-1}\right]\mathbf{L}_{i-1}^{\mu(1)}, \quad (43)$$

where the summation over complementary operators in the DMRG formalism (or the contraction of virtual bonds in the matrix product operator (MPO) formalism) is abbreviated as a multiplication symbol ($\times$). These equations are summarized diagrammatically in Fig. 3.

In Eq. (40), it should be noted that we use the projected coefficient

$$\tilde{\mathbf{C}}_i^{\mu(1)} = \mathbf{Q}_i^L\mathbf{C}_i^{\mu(1)} = \left(\mathbf{1} - \mathbf{L}_i^{(0)}\mathbf{L}_i^{(0)\dagger}\right)\mathbf{C}_i^{\mu(1)}, \quad (44)$$

to satisfy the left-fixed gauge condition of the first order wavefunction.

Similarly, the matrix elements of the projected overlap matrix $\mathbf{S}_R$ can be computed as

$$S_{\mu\nu} = \sum_{i=1}^{k} S^{[i]}_{\mu\nu} = \sum_{i=1}^{k}\tilde{\mathbf{C}}_i^{\mu(1)\dagger}\tilde{\mathbf{C}}_i^{\nu(1)}. \quad (45)$$

Note that any inter-site components of the overlap matrix vanish since $\mathbf{L}_i^{\mu(1)\dagger}\mathbf{L}_i^{(0)} = \mathbf{0}$.

C. Rotation of the first order vectors by the Ritz vectors

At the end of the sweep, we have the small generalized eigenvalue problem to solve

$$\mathbf{H}_R\boldsymbol{\alpha}_\mu = \omega_\mu\mathbf{S}_R\boldsymbol{\alpha}_\mu. \quad (46)$$

This gives an approximation of the excitation energy ω_μ and the Ritz vector $\boldsymbol{\alpha}_\mu$. The Ritz vector is then used to rotate the

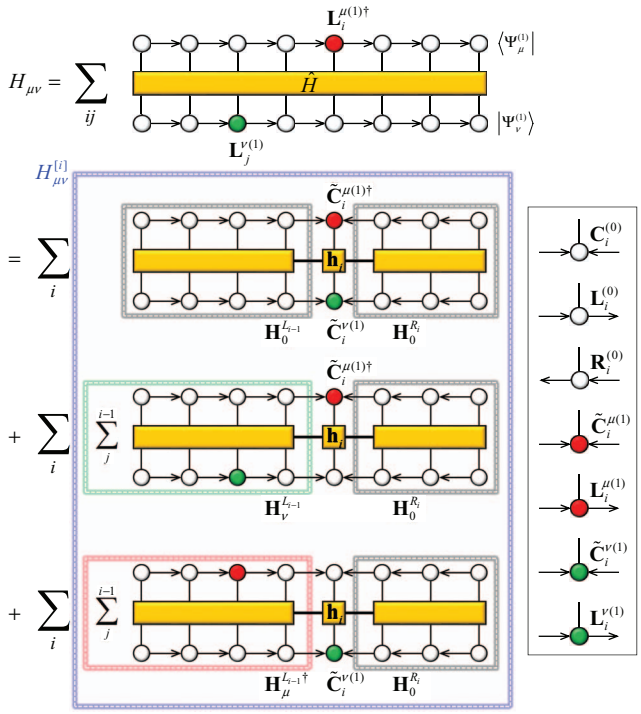

FIG. 3. Graphical summary for the computation of the projected Hamiltonian $H_{\mu\nu}$ in terms of the sweep algorithm.

first order objects to approximate the first order eigenstates,

$$\mathbf{L}_i^{\mu(1)} = \sum_{\mu'}\mathbf{L}_i^{\mu'(1)}\alpha_{\mu'\mu}, \qquad \mathbf{H}_\mu^{L_{i-1}} = \sum_{\mu'}\mathbf{H}_{\mu'}^{L_{i-1}}\alpha_{\mu'\mu}, \quad (47)$$

where μ' denotes the state index in the previous sweep. Note that the rotation performs the orthonormalization of trial vectors as well. Because the explicit orthonormalization of trial vectors, in principle, takes another sweep, it is advantageous to solve the small generalized eigenvalue problem so that the rotation and the orthonormalization can be done simultaneously.

As in the ground-state DMRG, sweeps are arranged as successive forward and backward iterations. In the forward sweep, for example, we only need to rotate the right-block objects (and vice versa in the backward sweep), i.e.,

$$\mathbf{R}_i^{\mu(1)} = \sum_{\mu'}\mathbf{R}_i^{\mu'(1)}\alpha_{\mu'\mu}, \qquad \mathbf{H}_\mu^{R_i} = \sum_{\mu'}\mathbf{H}_{\mu'}^{R_i}\alpha_{\mu'\mu}, \quad (48)$$

because the left-block objects such as $\mathbf{L}_{i-1}^{\mu(1)}$ and $\mathbf{H}_\mu^{L_{i-1}}$ have already been rotated at the previous site. These steps are illustrated diagrammatically in Fig. 4.

D. Davidson's correction equation

To compute the correction site-by-site, we consider the ith site component of the sigma-vector in the mixed-canonical

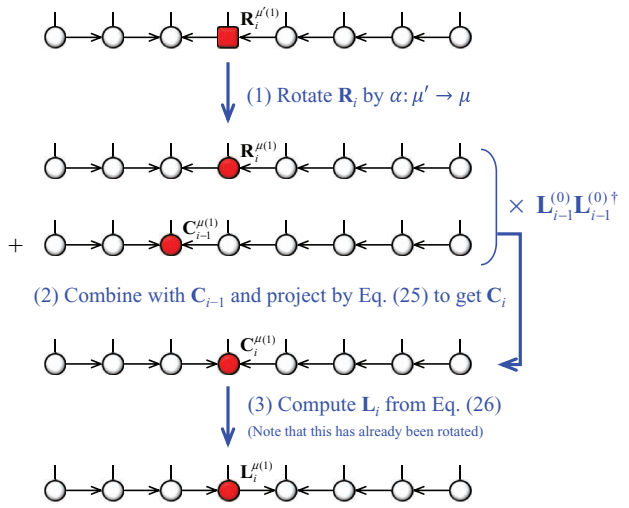

FIG. 4. Graphical summary for the Ritz vector rotation, gauge-transformation, and computation of the first order rotation matrix, through sweeping.

gauge

$$\boldsymbol{\sigma}^{\mu}_i = \mathbf{H}^{[i]}_0 \mathbf{C}^{\mu(1)}_i + \Delta\boldsymbol{\sigma}^{[i]}_{\mu} \mathbf{C}^{(0)}_i, \tag{49}$$

$$\begin{aligned}\Delta\boldsymbol{\sigma}^{[i]}_{\mu} = {} & \mathbf{H}^{L_{i-1}}_{\mu} \times \mathbf{h}_i \times \mathbf{H}^{R_i}_0 \\ & + \mathbf{H}^{L_{i-1}}_{0} \times \mathbf{h}_i \times \mathbf{H}^{R_i}_{\mu},\end{aligned} \tag{50}$$

where the first order right-renormalized operator $\mathbf{H}^{R_i}_{\mu}$ is given similarly to Eq. (43):

$$\begin{aligned}\mathbf{H}^{R_i}_{\mu} = {} & \mathbf{R}^{(0)}_{i+1}\left[\mathbf{H}^{R_{i+1}}_{\mu} \times \mathbf{h}_{i+1}\right]\mathbf{R}^{(0)\ \dagger}_{i+1} \\ & + \mathbf{R}^{(0)}_{i+1}\left[\mathbf{H}^{R_{i+1}}_{0} \times \mathbf{h}_{i+1}\right]\mathbf{R}^{\mu(1)\dagger}_{i+1}.\end{aligned} \tag{51}$$

The residual vector for each site $\mathbf{r}^{\mu}_i$ can then be computed as

$$\mathbf{r}^{\mu}_i = \boldsymbol{\sigma}^{\mu}_i - \omega_{\mu}\mathbf{C}^{\mu(1)}_i, \tag{52}$$

where we have assumed that the trial vectors are already rotated by the Ritz vectors. Note that $\mathbf{S}^{(0)}_{ij} = \mathbf{0}$ for $i \neq j$ and $\mathbf{S}^{(0)}_{ii} = \mathbf{1}$ in the mixed-canonical gauge at site i.

The correction for each site $\mathbf{z}_i$ is then computed as

$$\mathbf{z}^{\mu}_i = \mathbf{r}^{\mu}_i\left[\mathrm{diag.}(\mathbf{H}^{[i]}_0 - \omega_{\mu}\mathbf{1})\right]^{-1}, \tag{53}$$

in which the diagonal preconditioner is employed. Note that the diagonal block of the effective Hamiltonian $\mathbf{H}^{(0)}_{ii}$, in the mixed-canonical gauge, is equal to the zeroth order Hamiltonian $\mathbf{H}^{[i]}_0$ for the DMRG optimization.

Because $\mathbf{z}^{\mu}_i$ does not lie entirely in the null space of the zeroth order component, it is projected into the first order orthogonal subspace to yield a new trial vector:

$$\mathbf{C}^{m+\mu(1)}_i = \left(\mathbf{1} - \mathbf{C}^{(0)}_i\mathbf{C}^{(0)\dagger}_i\right)\mathbf{z}^{\mu}_i. \tag{54}$$

After this step, we continue the algorithm by approximating eigenstates in the larger trial space.

E. Generalization to DMRG-RPA

DMRG-RPA can be implemented with relatively minor modifications of DMRG-TDA.

Suppose we have m trial vectors $|\mathbf{X}^{\mu}, \mathbf{Y}^{\mu}\rangle$ with the approximate eigenvalues ω_{μ}. If these frequencies differ from zero, the vectors $|\mathbf{Y}^{\mu}, \mathbf{X}^{\mu}\rangle$ are also solutions, with the eigenvalues $-\omega_{\mu}$, due to the completeness of the RPA equation. The DMRG-RPA problem is then reduced to a $2m \times 2m$ non-hermitian eigenvalue problem spanned by the vectors $\{|\mathbf{X}^{\mu}, \mathbf{Y}^{\mu}\rangle, |\mathbf{Y}^{\mu}, \mathbf{X}^{\mu}\rangle\}$.[33]

The projected DMRG-RPA equation (27) is given by

$$\begin{pmatrix}\mathbf{H}_R & \mathbf{W}_R \\ \mathbf{W}^*_R & \mathbf{H}^*_R\end{pmatrix}\begin{pmatrix}\boldsymbol{\alpha}_X \\ \boldsymbol{\alpha}_Y\end{pmatrix} = \omega\begin{pmatrix}\mathbf{S}_R & \mathbf{D}_R \\ -\mathbf{D}^*_R & -\mathbf{S}^*_R\end{pmatrix}\begin{pmatrix}\boldsymbol{\alpha}_X \\ \boldsymbol{\alpha}_Y\end{pmatrix}, \tag{55}$$

in terms of the following $m \times m$ matrices:

$$H_{\mu\nu} = \begin{pmatrix}\mathbf{X}^{\mu} & \mathbf{Y}^{\mu}\end{pmatrix}\begin{pmatrix}\mathbf{H} & \mathbf{W} \\ \mathbf{W}^* & \mathbf{H}^*\end{pmatrix}\begin{pmatrix}\mathbf{X}^{\nu} \\ \mathbf{Y}^{\nu}\end{pmatrix}, \tag{56}$$

$$W_{\mu\nu} = \begin{pmatrix}\mathbf{X}^{\mu} & \mathbf{Y}^{\mu}\end{pmatrix}\begin{pmatrix}\mathbf{H} & \mathbf{W} \\ \mathbf{W}^* & \mathbf{H}^*\end{pmatrix}\begin{pmatrix}\mathbf{Y}^{\nu} \\ \mathbf{X}^{\nu}\end{pmatrix}, \tag{57}$$

$$S_{\mu\nu} = \begin{pmatrix}\mathbf{X}^{\mu} & \mathbf{Y}^{\mu}\end{pmatrix}\begin{pmatrix}\mathbf{S} & \mathbf{0} \\ \mathbf{0} & -\mathbf{S}^*\end{pmatrix}\begin{pmatrix}\mathbf{X}^{\nu} \\ \mathbf{Y}^{\nu}\end{pmatrix}, \tag{58}$$

$$D_{\mu\nu} = \begin{pmatrix}\mathbf{X}^{\mu} & \mathbf{Y}^{\mu}\end{pmatrix}\begin{pmatrix}\mathbf{S} & \mathbf{0} \\ \mathbf{0} & -\mathbf{S}^*\end{pmatrix}\begin{pmatrix}\mathbf{Y}^{\nu} \\ \mathbf{X}^{\nu}\end{pmatrix}. \tag{59}$$

The rotation of the first order vectors by the Ritz vectors has to be carried out for the forward and backward propagating parts $\{\boldsymbol{\alpha}_X, \boldsymbol{\alpha}_Y\}$ simultaneously:

$$\begin{aligned}\mathbf{X}^{\mu}_i &= \sum_{\mu'}\left(\mathbf{X}^{\mu'}_i\alpha_{X,\mu'\mu} + \mathbf{Y}^{\mu'}_i\alpha_{Y,\mu'\mu}\right), \\ \mathbf{Y}^{\mu}_i &= \sum_{\mu'}\left(\mathbf{Y}^{\mu'}_i\alpha_{X,\mu'\mu} + \mathbf{X}^{\mu'}_i\alpha_{Y,\mu'\mu}\right).\end{aligned} \tag{60}$$

To compute the second order derivative contributions in the $\mathbf{W}$ matrix, the non-redundant parameterization is performed by taking the projection $\mathbf{Q}^L_i \times \mathbf{Q}^R_j : (i < j)$, as discussed before.

For example, the non-redundant contribution coming from a pair of nearest neighbour sites $\mathbf{C}^{(1)}_i\mathbf{R}^{(1)}_{i+1}$ is obtained as

$$\mathbf{Q}^L_i\mathbf{C}^{(1)}_i\mathbf{R}^{(1)}_{i+1}\mathbf{Q}^R_{i+1} = \mathbf{L}^{(1)}_i\boldsymbol{\Lambda}_i\mathbf{R}^{(1)}_{i+1}. \tag{61}$$

For the next nearest neighbour sites as

$$\mathbf{Q}^L_{i-1}\mathbf{C}^{(1)}_i\mathbf{R}^{(0)}_i\mathbf{R}^{(1)}_{i+1}\mathbf{Q}^R_{i+1} = \mathbf{L}^{(1)}_{i-1}\mathbf{C}^{(0)}_i\mathbf{R}^{(1)}_{i+1}, \tag{62}$$

and so forth.

To take these second order changes into account, the matrix elements $W_{\mu\nu}$ are computed as

$$\begin{aligned}W_{\mu\nu} &= \sum_i W^{[i]}_{\mu\nu} \\ &= \sum_i\left(\boldsymbol{\Lambda}_i\mathbf{R}^{\mu(1)}_i\right)^{\dagger}\Delta\mathbf{H}^{[i]\dagger}_{\nu}\mathbf{C}^{(0)}_i + \left(\boldsymbol{\Lambda}_i\mathbf{R}^{\nu(1)}_i\right)^{\dagger}\Delta\mathbf{H}^{[i]\dagger}_{\mu}\mathbf{C}^{(0)}_i,\end{aligned} \tag{63}$$

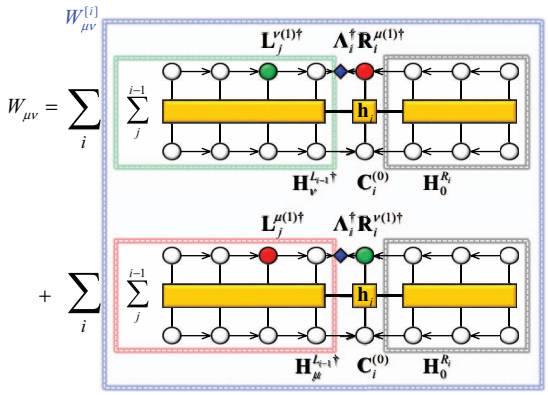

FIG. 5. Graphical representation for computation of $W^{[i]}_{\mu\nu}$.

where $\Delta\mathbf{H}^{[i]}_\nu$ is the same as Eq. (42), but now the conjugate is considered. Note that the matrix elements of $\mathbf{W}$ have to be computed through two sweeps because they depend on both $\mathbf{L}_i^{(1)}$ and $\mathbf{R}_i^{(1)}$, which are obtained from forward and backward sweeps, respectively. The computation of $W_{\mu\nu}$ is illustrated diagrammatically in Fig. 5

IV. PSEUDOCODE FOR DMRG-TDA/RPA

In Fig. 6, we summarize our DMRG-TDA algorithm to target the n lowest excited states as a pseudocode. All zeroth order information, $\{\mathbf{L}_i^{(0)}, \mathbf{C}_i^{(0)}, \mathbf{R}_i^{(0)}\}$, $\mathbf{H}_i^{L_i}$, and $\mathbf{H}_i^{R_i}$, is supposed to be known from the ground-state DMRG calculation. The overall complexity of our algorithm is $\mathcal{O}(dM^3k^3N + dM^2kN^2)$, where N is the maximum number of trial vectors in the Davidson algorithm. We have implemented these DMRG-TDA and DMRG-RPA algorithms into our spin-adapted DMRG code (BLOCK).[5,12,13]

choose n trial vectors $\{\mathbf{X}_\mu : 1 \le \mu \le n\}$
$m \leftarrow n$
loop ▷ Iteration for the Davidson Algorithm
  solve $\mathbf{H}_R \boldsymbol{\alpha}_\mu = \omega_\mu \mathbf{S}_R \boldsymbol{\alpha}_\mu$
  $l \leftarrow m + n$
  $H_{\mu\nu} \leftarrow 0, S_{\mu\nu} \leftarrow 0 : \mu, \nu = 1, \ldots, l$
  $r_\mu^2 \leftarrow 0$
  for $i = 1 \to k$ **do** ▷ Start Forward Sweep
    for $\mu = 1 \to m$ **do**
      $\mathbf{R}_i^{\mu(1)}, \mathbf{H}_\mu^{R_i} \leftarrow$ Eq. (48)
      $\mathbf{C}_i^{\mu(1)} \leftarrow$ Eq. (25)
    end for
    for $\mu = 1 \to n$ **do**
      $\sigma_i^\mu \leftarrow$ Eq. (49)
      $\mathbf{r}_i^\mu \leftarrow$ Eq. (52)
      $\mathbf{C}_i^{m+\mu(1)} \leftarrow$ Eq. (54)
      $r_\mu^2 \leftarrow r_\mu^2 + |\mathbf{r}_i^\mu|^2$
    end for
    for $\mu = 1 \to l$ **do**
      $\tilde{\mathbf{C}}_i^{\mu(1)} \leftarrow$ Eq. (44)
    end for
    for $\mu = 1 \to l$ **do**
      for $\nu = 1 \to l$ **do**
        $H_{\mu\nu} \leftarrow H_{\mu\nu} + H^{[i]}_{\mu\nu}$ ▷ Eq. (40)
        $S_{\mu\nu} \leftarrow S_{\mu\nu} + S^{[i]}_{\mu\nu}$ ▷ Eq. (45)
      end for
    end for
    for $\mu = 1 \to l$ **do**
      $\mathbf{L}_i^{\mu(1)} \leftarrow$ Eq. (26)
      $\mathbf{H}_\mu^{L_i} \leftarrow$ Eq. (43)
    end for
  end for ▷ End Forward Sweep
  for $i = k \to 1$ **do** ▷ Start Backward Sweep
    for $\mu = 1 \to l$ **do**
      $\mathbf{R}_i^{\mu(1)} \leftarrow$ Eq. (24)
      $\mathbf{H}_\mu^{R_{i-1}} \leftarrow$ Eq. (51)
    end for
  end for ▷ End Backward Sweep
  if $\{|\mathbf{r}_\mu|^2 < \epsilon : 1 \le \mu \le n\}$ **then**
    Exit on Convergence
  end if
  if $l < N$ **then**
    $m \leftarrow l$
  else
    $m \leftarrow n$ ▷ Deflation
  end if
end loop

FIG. 6. Pseudocode for the DMRG-TDA calculation of the n lowest excited states. The zeroth order components $\mathbf{L}_i^{(0)}$, $\mathbf{C}_i^{(0)}$, and $\mathbf{R}_i^{(0)}$ are assumed to be solved and stored. The μth trial vector $\mathbf{X}_\mu$ consists of a set of first order changes $\mathbf{L}_i^{\mu(1)}$, $\mathbf{C}_i^{\mu(1)}$, and $\mathbf{R}_i^{\mu(1)}$. The first order right-block objects, $\mathbf{H}_R$ and $\mathbf{S}_R$, are assumed to be computed for the first n trial vectors before the algorithm starts. The initial trial vectors are random. The real (and small) number ϵ gives the threshold for convergence.

V. QUALITATIVE UNDERSTANDING OF DMRG-LRT EXCITATIONS

Before proceeding to numerical applications, we briefly discuss the physics of excitations that appear in DMRG-TDA and DMRG-RPA. It is not immediately straightforward to link site-based excitation theories (such as DMRG-TDA and DMRG-RPA) to standard chemical intuition, which is formulated in terms of particle-based excitations. A site-based excitation hierarchy will efficiently capture certain kinds of high-particle rank excitations (that are difficult to describe in particle-based theories), while poorly describing other kinds of excitations with low-particle rank character. While both DMRG-TDA and DMRG-RPA are formally exact as $M \to \infty$, the rate of convergence for different kinds of excited states may nonetheless be very different.

Generically, we can write an exact excited state $|\Psi'\rangle$ as an operator $\hat{\Omega}$ acting on the exact ground-state $|\Psi_0\rangle$,

$$|\Psi'\rangle = \hat{\Omega}\,|\Psi_0\rangle = \sum_i c_i \hat{O}_i\,|\Psi_0\rangle\,. \tag{64}$$

If one approximates $|\Psi_0\rangle$ by an approximate ground state, this gives rise to an ansatz for excited states with a long history, known historically both as the Feynman–Bijl ansatz,[34,35] and the single mode approximation.[36] In quantum chemistry this is the basis of "internally contracted" methods for excitations, such as internally contracted multi-reference configuration interaction, and equation of motion coupled cluster, where $\hat{O}_i$ are the excitation operators.

An approximate particle-based excitation theory, such as EOM-CCSD, based on a Hartree-Fock ground-state $|\Phi_0\rangle$, performs well if $\hat{O}_i$ are low-rank particle operators (such as single-particle excitation operators) *and* if $||\hat{O}_i(|\Psi_0\rangle - |\Phi_0\rangle)||$ is small. The latter is not true if $\hat{O}_i$ annihilates $|\Phi_0\rangle$, which will happen if $\hat{O}_i$ is a virtual to virtual excitation, since virtuals are not occupied in the ground-state. Such excited states must then be described using a higher-rank excitation operator, even if the *exact* excitation operator $\hat{\Omega}$ is in fact low-rank.

DMRG-TDA and DMRG-RPA on the other hand, perform well when the $\hat{O}_i$ are operators that act only on a small number of neighbouring sites on the DMRG mapping to a 1D lattice, as discussed extensively in Refs 25, 27, and 37. Since multi-particle operators (such as $\hat{n}_\alpha \hat{n}_\beta$) can be defined even for a single site, this means that certain kinds of multi-particle excitations may be efficiently captured.

Singly excited states can be obtained using an excitation of the form $\sum_{ij} C_{ij} \hat{a}_i^\dagger \hat{a}_j$ where i, j denote local sites. This implies that DMRG-TDA and DMRG-RPA are most efficient when the bandwidth of C_{ij} is small, which is the case for tightly bound excitons. Similarly $\hat{O}_i$ should not annihilate the approximate DMRG ground-state, which can happen if the approximate ground-state does not populate some quantum number sectors at certain lattice partitions, which are involved in the exact excitation operator (similar to certain orbitals not being occupied in the ground state). We will see examples of this in the calculations that follow.

VI. ILLUSTRATIVE APPLICATIONS

In this section, we present *ab initio* DMRG-TDA benchmark calculations on molecular systems, and compare them to SA-DMRG and other conventional methods. Since we previously reported DMRG-RPA benchmark calculations for the Hubbard and Pariser-Parr-Pople (PPP) model Hamiltonians,[26] here we only focus on DMRG-TDA.

First, we compute the low-lying excited states of polyenes. DMRG works very well for this type of molecule. Single-reference theories, in contrast, fail due to the doubly excited configurations which appear both in the ground and excited states.

Second, we consider the excited states of the water molecule to investigate the performance of DMRG-TDA for more general non-one-dimensional molecules.

Finally, we test the performance of DMRG-TDA for a highly complex system, the [2Fe-2S] iron-sulfur cluster. It is very difficult to accurately investigate this cluster with conventional theories, due to the near-degeneracy of ground and excited states.

A. Low-lying excited states of polyenes

Low-lying excited states of polyenes are of interest because the doubly excited A_g state appears to cross the first B_u state in longer polyenes. With increasing chain length, the energy gap between the ground state and these excited states becomes smaller, and doubly excited configurations start to mix into the ground state. Non-dynamical electron correlation is therefore important in long polyene molecules. It is well established that DMRG performs well for such a non-dynamical electron correlation, and hence polyene molecules.

We carried out DMRG-TDA and SA-DMRG calculations for the lowest 8 excited states of C_nH_{n+2}, where $n = 4$, 8, 12, 16, 20, and 24. Geometries were taken to be all-trans and were optimized at the B3LYP/cc-pVDZ level of theory. Molecular orbitals were computed at the RHF/cc-pVDZ level of theory, and localized for occupied and unoccupied spaces separately. The active space was chosen to be π-double valence, i.e., n π-electrons in $2n$ π-orbitals, where n is the number of carbon atoms.

To investigate the convergence of energies with M, we performed DMRG-TDA and 8SA-DMRG calculations on C_8H_{10} and $C_{16}H_{18}$ with $M = 50$, 100, 150, and 200. The energy errors from the converged calculations are summarized in Tables I and II (see also Figures 7 and 8). From these results we can infer that DMRG-TDA gives faster convergence in the small M region (up to $M = 100$), but slower convergence in the large M region, as compared to 8SA-DMRG. DMRG-TDA works better in the region where M is not sufficiently large to describe the ground and excited states simultaneously with SA-DMRG. In contrast, SA-DMRG can describe higher order excitations from the ground state for which DMRG-TDA converges slow with M. An example of this is the $3A_g$ state of $C_{16}H_{18}$. We conclude that this state involves multi-site excitations in the DMRG chain.

To help analyze the nature of the excited states, we have computed the one-particle transition density matrix

$$\gamma^\nu_{pq} = \langle \Psi^\nu | \hat{a}_p^\dagger \hat{a}_q | \Psi_0 \rangle \,, \tag{65}$$

and its square norm $\sum_{pq} (\gamma^\nu_{pq})^2$ is summarized in Table III. These square norms show that the $3B_u$ state consists of a single-particle excitation, while the $3A_g$ and $4B_u$ states have a large multi-particle excitation character. Some correlation between the square norms and the errors of DMRG-TDA can be deduced for the polyenes: if the single-particle character of the excitation is large, a single-site excitation (DMRG-TDA) describes it well, and vice versa. Thus in the polyenes, DMRG-TDA works well unless the single-particle character is completely lost. This is consistent with the physics of polyenes: the single excited states, due to the poorly screened Coulomb interaction, consist of strongly bound charged quasiparticles (and are thus linear combinations of "local" site excitations) while the doubly excited states consist of weakly bound neutral (triplet excitation) quasiparticles[38] (and thus involve two independent "local" excitations, which cannot be captured well in a single-site picture).

We also investigated the change of the excitation energies with elongation of the polyene chain. Fig. 9 shows how the energy of the lowest 2 singlet excited states and the lowest

TABLE I. Energy errors in mE_h for the C_8H_{10} molecule, computed by 8SA-DMRG and DMRG-TDA with $M = 50$, 100, 150, and 200. The converged energy $E_{\text{conv.}}$ is computed by an 8SA-DMRG calculation with $M = 1000$.

		$M = 50$		$M = 100$		$M = 150$		$M = 200$	
State	$E_{\text{conv.}}/E_h$	SA	TDA	SA	TDA	SA	TDA	SA	TDA
XA_g	−308.839 603	0.28	0.01	0.05	0.00	0.01	0.00	0.00	0.00
$2A_g$	−308.662 869	1.58	1.13	0.11	0.12	0.02	0.07	0.01	0.03
$1B_u$	−308.621 251	1.21	0.41	0.11	0.07	0.02	0.04	0.01	0.01
$2B_u$	−308.610 083	1.17	0.22	0.17	0.03	0.03	0.01	0.01	0.00
$3A_g$	−308.597 039	0.94	0.51	0.11	0.10	0.02	0.05	0.01	0.03
$4A_g$	−308.560 117	2.81	14.90	0.15	2.23	0.04	1.15	0.01	0.62
$3B_u$	−308.534 448	1.71	1.63	0.14	0.25	0.03	0.14	0.01	0.13
$5A_g$	−308.528 264	1.02	0.13	0.14	0.04	0.03	0.03	0.01	0.03

TABLE II. Energy errors in mE_h for the $C_{16}H_{18}$ molecule, computed by 8SA-DMRG and DMRG-TDA with $M = 50$, 100, 150, and 200. The converged energy $E_{\text{conv.}}$ is computed by an 8SA-DMRG calculation with $M = 1000$.

		$M = 50$		$M = 100$		$M = 150$		$M = 200$	
State	$E_{\text{conv.}}/E_h$	SA	TDA	SA	TDA	SA	TDA	SA	TDA
XA_g	− 616.536 393	2.24	0.13	0.56	0.02	0.21	0.01	0.09	0.00
$2A_g$	− 616.415 267	10.78	6.41	1.56	1.41	0.50	0.91	0.23	0.71
$1B_u$	− 616.388 094	9.39	4.32	1.44	0.80	0.52	0.48	0.24	0.34
$2B_u$	− 616.362 242	8.28	3.01	1.41	0.52	0.53	0.30	0.24	0.21
$3B_u$	− 616.357 091	9.16	1.79	2.11	0.34	0.72	0.16	0.34	0.11
$3A_g$	− 616.352 480	19.75	15.46	2.83	13.78	0.79	13.49	0.38	11.57
$4A_g$	− 616.339 250	7.54	20.53	1.64	3.85	0.66	0.45	0.30	0.30
$4B_u$	− 616.326 394	13.34	21.11	2.69	6.16	0.84	5.95	0.41	5.93

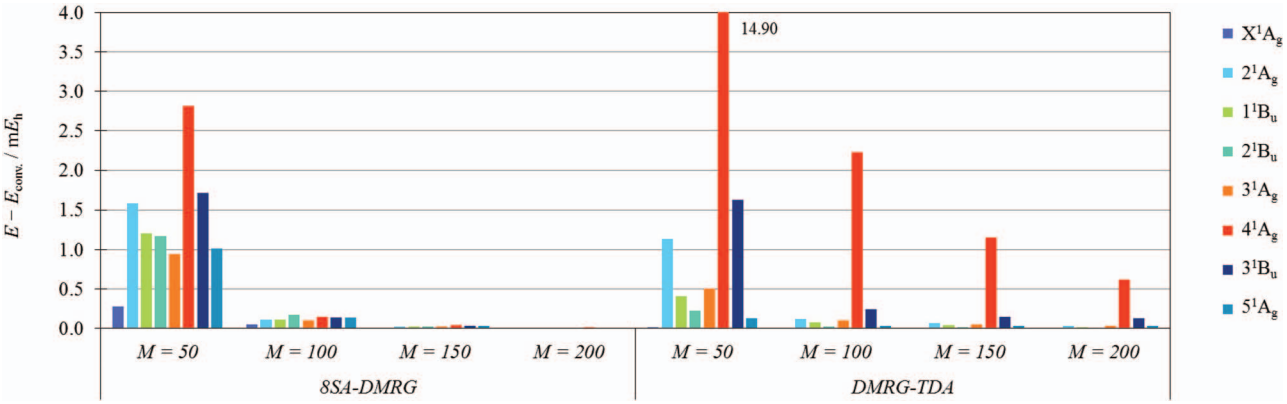

FIG. 7. Energy errors in mE_h for the C_8H_{10} molecule; a graphical summary for Table I.

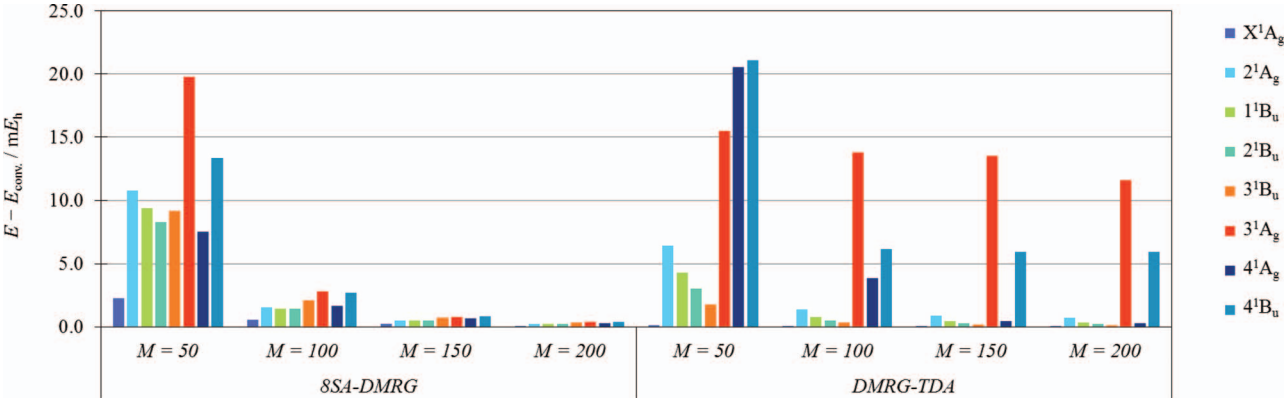

FIG. 8. Energy errors in mE_h for the $C_{16}H_{18}$ molecule; a graphical summary for Table II.

TABLE III. Square norm of one-particle transition density matrix $\sum_{pq} \gamma_{pq}^2$ compared to the errors in the DMRG-TDA calculations for $C_{16}H_{18}$ (ΔE in mE_h) with $M = 200$.

State	$\sum_{pq} \gamma_{pq}^2$	ΔE
$2A_g$	0.507	0.71
$1B_u$	0.533	0.34
$2B_u$	0.566	0.21
$3B_u$	1.570	0.11
$3A_g$	0.266	11.57
$4A_g$	0.611	0.30
$4B_u$	0.246	5.93

3 triplet excited states changes, as computed by DMRG-TDA with $M = 200$. The curves agree with previous studies,[38–40] and it can therefore be concluded that DMRG-TDA correctly describes the low-lying excited states of polyene molecules.

B. Water molecule

The water molecule is often used as a benchmark system for excited state theories. Here, we present the lowest 12 excited states computed by DMRG-TDA, SA-DMRG, and EOM-CCSD with the cc-pVDZ and aug-cc-pVDZ basis sets. The calculations were carried out with the equilibrium geometry; R(OH) = 1.8111a_{Bohr} and ∠HOH = 104.45°. The active spaces we employed were 8 electrons in 23 orbitals and 8 electrons in 40 orbitals, for the cc-pVDZ and aug-cc-pVDZ basis sets, respectively. The 1s core orbitals were kept frozen. We performed the DMRG-TDA and 4SA-DMRG calculations with $M = 500$, for each irreducible symmetry. It should be noted that the reference states were computed separately for each state symmetry in the DMRG-TDA calculation, because a symmetry changing deviation cannot always be captured by "single-site" excitation, due to missing quantum numbers in the ground state as discussed earlier (also see below).

Energies of the ground and lowest 12 excited states are summarized in Tables IV and V. With the cc-pVDZ basis set, both the DMRG-TDA and 4SA-DMRG energies are converged at $M = 500$, except for the $4A_1$ state with DMRG-TDA. With the larger aug-cc-pVDZ basis set, the 4SA-DMRG numbers exhibit systematic errors on the order of 2 mE_h, while the DMRG-TDA numbers are generally better than the 4SA-DMRG numbers, except for a few states. The errors for DMRG-TDA are however not systematic, indicating that DMRG-TDA breaks down for some specific cases, e.g., $2A_1$ and $3A_1$ states. These states cannot be described in terms of a "single-site" excitation.

The EOM-CCSD energies mostly agree with the converged energies on the order of 3 mE_h, but some higher energy states are missing with the cc-pVDZ basis set. These high

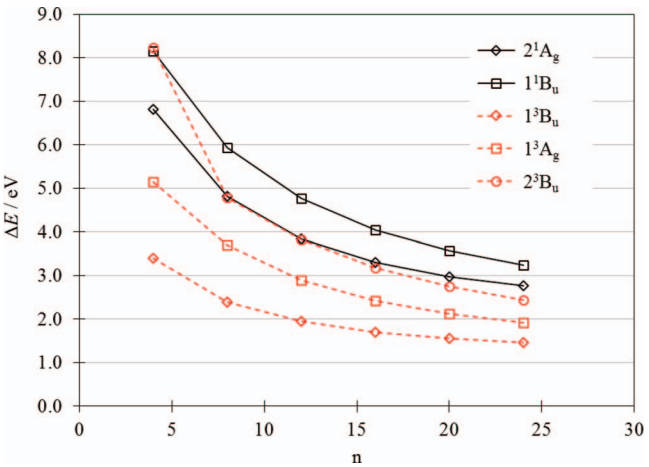

FIG. 9. Changes of excitation energy in eV for the 2^1A_g, 1^1B_u, 1^3B_u, 1^3A_g, and 2^3B_u states of polyene molecules C_nH_{n+2} where n ranges from 4 to 24.

TABLE IV. Energies of the ground and the lowest 12 excited states of the water molecule as computed by 4SA-DMRG ($M = 500$), DMRG-TDA ($M = 500$), and EOM-CCSD, in the cc-pVDZ basis set. Note that the DMRG-TDA and SA-DMRG calculations were carried out for each irreducible representation separately.

	$E_{\text{conv.}}/E_h$	$E - E_{\text{conv.}}$/mE_h		
State	4SA $M = 2000$	4SA $M = 500$	TDA $M = 500$	EOM-CCSD
XA_1	−76.241 697	0.11	0.01	3.68
$1B_1$	−75.939 176	0.20	0.02	1.50
$1A_2$	−75.864 445	0.20	0.02	2.07
$2A_1$	−75.842 487	0.18	0.12	2.08
$1B_2$	−75.765 964	0.21	0.02	2.55
$2B_2$	−75.696 018	0.20	0.45	4.14
$3A_1$	−75.584 080	0.16	0.10	5.13
$4A_1$	−75.462 977	0.26	2.69	N/A
$2A_2$	−75.448 180	0.23	0.04	4.53
$3A_2$	−75.403 286	0.33	0.27	N/A
$2B_1$	−75.401 515	0.28	0.25	24.20
$3B_1$	−75.381 977	0.26	0.07	N/A
$3B_2$	−75.322 655	0.26	0.07	5.75

TABLE V. Energies of the ground and the lowest 12 excited states of the water molecule as computed by 4SA-DMRG ($M = 500$), DMRG-TDA ($M = 500$), and EOM-CCSD, in the aug-cc-pVDZ basis set. Note that the DMRG-TDA and SA-DMRG calculations were carried out for each irreducible representation separately.

	$E_{\text{conv.}}/E_h$	$E - E_{\text{conv.}}$/mE_h		
State	4SA $M = 2000$	4SA $M = 500$	TDA $M = 500$	EOM-CCSD
XA_1	−76.274 423	1.29	0.31	5.86
$1B_1$	−75.997 383	2.04	0.49	2.66
$1A_2$	−75.931 824	1.91	0.43	1.96
$2A_1$	−75.909 074	2.17	11.51	2.84
$2B_1$	−75.863 101	2.02	1.47	2.10
$1B_2$	−75.844 352	2.06	0.42	1.97
$3A_1$	−75.839 232	2.46	4.47	2.63
$3B_1$	−75.833 279	2.13	0.54	2.30
$2A_2$	−75.826 508	2.02	0.54	3.41
$3A_2$	−75.788 484	2.02	0.49	1.29
$4B_1$	−75.770 624	3.14	11.36	2.14
$4A_1$	−75.766 827	2.27	9.44	2.37
$2B_2$	−75.762 108	2.00	17.53	3.89

TABLE VI. Energies of the ground and the lowest 12 excited states of the water molecule as computed by 8SA-DMRG ($M = 500$), 13SA-DMRG ($M = 500$), and DMRG-TDA ($M = 500$) in the cc-pVDZ basis set, where the valence molecular orbitals were localized. The 4SA $M = 2000$ results were taken from Table IV.

	$E_{\text{conv.}}/E_h$	$E - E_{\text{conv.}}/\text{m}E_h$		
State	4SA $M = 2000$	8SA $M = 500$	13SA $M = 500$	TDA $M = 500$
XA_1	−76.241 697	1.62	3.01	0.24
$1B_1$	−75.939 176	2.11	3.37	1.20
$1A_2$	−75.864 445	2.71	4.05	2.78
$2A_1$	−75.842 487	1.68	3.11	0.43
$1B_2$	−75.765 964	1.96	3.64	0.57
$2B_2$	−75.696 018	1.47	2.90	0.29
$3A_1$	−75.584 080	2.10	4.13	0.39
$4A_1$	−75.462 977	2.86	4.77	4.89
$2A_2$	−75.448 180	...	6.78	N/A
$3A_2$	−75.403 286	...	5.50	5.39
$2B_1$	−75.401 515	...	4.31	5.37
$3B_1$	−75.381 977	...	7.90	N/A
$3B_2$	−75.322 655	...	7.00	6.98

energy states, which have high particle-rank character, are nonetheless correctly described by DMRG-TDA. Conversely EOM-CCSD works very well for certain singly excited states for which DMRG-TDA breaks down. This illustrates the fact that single-site and single-particle excitations are in general of fundamentally different character.

We also present DMRG-TDA results when the valence orbitals are localized, as summarized in Table VI. In this calculation, the A_1 ground state was chosen as the reference for all excited states, i.e., symmetry changing excitations were considered. DMRG-TDA works better than SA-DMRG if localized orbitals are used instead of canonical orbitals, for most of the low-lying excited states of the water molecule. However, there are larger errors in high energy states and some missing excited states. This indicates that symmetry changing excitations cannot always be represented by single-site excitations because the ground-state may be missing quantum numbers important to the symmetry change.

C. $[Fe_2S_2(SCH_3)_4]^{3-}$ cluster

The [2Fe-2S] iron-sulfur clusters are found in various classes of oxidoreductase enzymes, which mediate electron transfer from a redox molecule such as NAD^+/NADH to the enzyme reaction center.

Recently, a high-accuracy DMRG calculation on such an iron-sulfur cluster was performed and helped to clarify the ground state electronic structure of the complicated cluster.[13] The excited states of the iron-sulfur cluster are also interesting, since the ground and excited states are expected to be highly degenerate. Here, we demonstrate the performance of SA-DMRG and DMRG-TDA for the large number of quasi-degenerate excited states.

Geometry, basis sets, and active space were taken from the earlier DMRG work.[13] We focused on the doublet, quartet, sextet, and octet spin states and computed the lowest 10 states for each spin state.

TABLE VII. Excitation energies in eV of the lowest 10 states for the doublet, quartet, sextet, and octet spin states, computed by 10SA-DMRG and DMRG-TDA with $M = 500$. The active space involves 3d orbitals of the iron centers and 3p orbitals of the sulfur atoms, except for the non-bonding orbitals. In total, it consists of 31 electrons in 20 orbitals. The ground state is in the doublet spin state.

	10SA-DMRG ($M = 500$)				DMRG-TDA ($M = 500$)			
State	Doublet	Quartet	Sextet	Octet	Doublet	Quartet	Sextet	Octet
1A	0.00	0.02	0.06	0.09	0.00	0.02	0.05	0.10
2A	0.04	0.06	0.08	0.13	0.03	0.06	0.07	0.14
3A	0.14	0.17	0.28	0.44	0.14	0.16	0.28	0.45
4A	0.31	0.46	0.52	0.59	0.31	0.46	0.52	0.59
5A	0.45	0.48	0.53	0.62	0.45	0.48	0.53	0.63
6A	0.52	0.51	0.57	0.68	0.52	0.51	0.56	0.69
7A	0.54	0.52	0.68	0.95	0.54	0.51	0.68	0.96
8A	0.54	0.66	0.82	1.02	0.54	0.65	0.81	1.04
9A	0.67	0.80	0.96	1.03	0.68	0.80	0.96	1.04
10A	0.71	0.85	1.03	1.11	0.72	0.86	1.03	1.17

Table VII summarizes the excitation energies of the $[Fe_2S_2(SCH_3)_4]^{3-}$ cluster. The SA-DMRG and DMRG-TDA energies are very close to each other, which implies that for this molecule SA-DMRG surprisingly works as well as DMRG-TDA, despite the averaging over many states. It indicates that the renormalized basis necessary for a good ground-state description, is also relevant for the excited states.

The excited states of $[Fe_2S_2(SCH_3)_4]^{3-}$ are very close to the ground state, and conventional single reference theories have great difficulty in describing such a system due to the serious quasi-degeneracy (see Fig. 10). It is interesting to see that only "single-site" excitations from the DMRG reference wavefunction are sufficient to compute these complicated excited states.

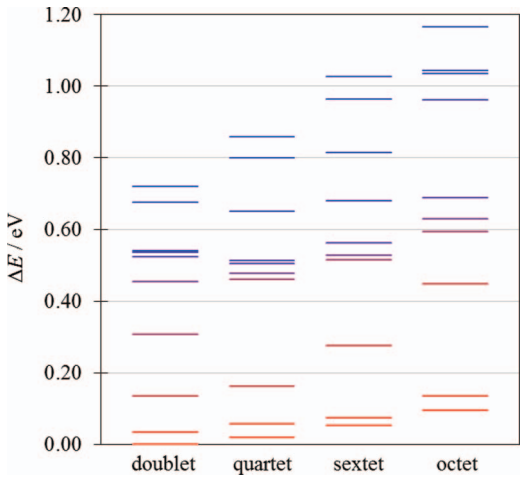

FIG. 10. Excitation energies in eV of the lowest 10 states for the doublet, quartet, sextet, and octet spin states, computed by DMRG-TDA with $M = 500$. See also Table VII for more detailed data.

VII. SUMMARY

In this work, we discussed in detail two post-density matrix renormalization group, namely, the DMRG analogue of the Tamm-Dancoff Approximation (DMRG-TDA) and the DMRG analogue of the Random Phase Approximation (DMRG-RPA), which were introduced both in our earlier work (Ref. 26) and the work of Haegeman *et al.* (Ref. 27). These methods provide new routes to excited states within DMRG. Both can be derived from our earlier linear response theory for the DMRG (Ref. 21). One of the main purposes of this work was to present an efficient sweep algorithm to solve for excited states in the DMRG-TDA and DMRG-RPA equations. The algorithm we presented may be easily implemented within any existing DMRG code, thus opening up the simple adoption of these techniques.

We further presented benchmark calculations on a number of *ab initio* model systems: polyenes, the water molecules, and a [2Fe-2S] cluster. These calculations provide insight into the "single-site" nature of excitations in DMRG-TDA; single-site meaning that the excitation is generated by a sum of operators, each acting on a single site or small number of consecutive sites in the DMRG lattice. In particular, single-*site* excitations do not generally correspond to single-*particle* excitations in particle-based theories. Rather, some many-particle excitations are easily described with single-site excitations, while other single-particle excitations are hard to describe. DMRG-TDA (and DMRG-RPA) thus offer a complementary approach to excited states, as compared to standard particle-based theories. Whether or not an excited state is well described by DMRG-TDA also provides useful physical insight. For example, in the case of polyenes, DMRG-TDA provided a good description of singly excited states and a poor description of doubly excited states, suggesting that singly excited states consist of strongly bound quasi-particles, while the doubly excited states consist of weakly bound quasi-particles.

The DMRG-TDA and DMRG-RPA methods discussed here are the lowest rung on a more general hierarchy of post-DMRG methods discussed in Ref. 26. Their success and complementary nature to standard particle-based mean-field hierarchies provides further motivation to explore higher rungs on the post-DMRG ladder.

ACKNOWLEDGMENTS

N.N. would like to thank Dr. Sandeep Sharma for his help on the computations of the iron-sulfur cluster. S.W. acknowledges funding from the Research Foundation Flanders. This work was supported by the National Science Foundation (NSF) through Grant Nos. NSF:SSI-SSE, OCI-1265278, and NSF:CHE-1265277.

[1] S. R. White, Phys. Rev. Lett. **69**, 2863 (1992).
[2] S. R. White, Phys. Rev. B **48**, 10345 (1993).
[3] S. R. White and R. L. Martin, J. Chem. Phys. **110**, 4127 (1999).
[4] A. O. Mitrushenkov, G. Fano, F. Ortolani, R. Linguerri, and P. Palmieri, J. Chem. Phys. **115**, 6815 (2001).
[5] G. K.-L. Chan and M. Head-Gordon, J. Chem. Phys. **116**, 4462 (2002).
[6] O. Legeza, J. Röder, and B. A. Hess, Phys. Rev. B **67**, 125114 (2003).
[7] G. Moritz and M. Reiher, J. Chem. Phys. **126**, 244109 (2007).
[8] D. Zgid and M. Nooijen, J. Chem. Phys. **128**, 014107 (2008).
[9] Y. Kurashige and T. Yanai, J. Chem. Phys. **130**, 234114 (2009).
[10] K. H. Marti and M. Reiher, Z. Phys. Chem. **224**, 583 (2010).
[11] H.-G. Luo, M.-P. Qin, and T. Xiang, Phys. Rev. B **81**, 235129 (2010).
[12] G. K.-L. Chan and S. Sharma, Annu. Rev. Phys. Chem. **62**, 465 (2011).
[13] S. Sharma and G. K.-L. Chan, J. Chem. Phys. **136**, 124121 (2012).
[14] S. Wouters, P. A. Limacher, D. Van Neck, and P. W. Ayers, J. Chem. Phys. **136**, 134110 (2012).
[15] S. Östlund and S. Rommer, Phys. Rev. Lett. **75**, 3537 (1995).
[16] S. Rommer and S. Östlund, Phys. Rev. B **55**, 2164 (1997).
[17] F. Verstraete, V. Murg, and J. Cirac, Adv. Phys. **57**, 143 (2008).
[18] U. Schollwöck, Ann. Phys. **326**, 96 (2011).
[19] B. O. Roos, "The complete active space self-consistent field method and its applications in electronic structure calculations," in *Advances in Chemical Physics* (John Wiley & Sons, Inc., 2007), pp. 399–445.
[20] J. J. Dorando, J. Hachmann, and G. K.-L. Chan, J. Chem. Phys. **127**, 084109 (2007).
[21] J. J. Dorando, J. Hachmann, and G. K.-L. Chan, J. Chem. Phys. **130**, 184111 (2009).
[22] J. M. Kinder, C. C. Ralph, and G. K.-L. Chan, "Analytic Time Evolution, Random Phase Approximation, and Green Functions for Matrix Product States," preprint arXiv:1103.2155 [cond-mat.str-el] (2011).
[23] J. Haegeman, J. I. Cirac, T. J. Osborne, I. Pižorn, H. Verschelde, and F. Verstraete, Phys. Rev. Lett. **107**, 070601 (2011).
[24] B. Pirvu, J. Haegeman, and F. Verstraete, Phys. Rev. B **85**, 035130 (2012).
[25] J. Haegeman, B. Pirvu, D. J. Weir, J. I. Cirac, T. J. Osborne, H. Verschelde, and F. Verstraete, Phys. Rev. B **85**, 100408(R) (2012).
[26] S. Wouters, N. Nakatani, D. Van Neck, and G. K.-L. Chan, Phys. Rev. B **88**, 075122 (2013).
[27] J. Haegeman, T. J. Osborne, and F. Verstraete, Phys. Rev. B **88**, 075133 (2013).
[28] G. K.-L. Chan, Phys. Chem. Chem. Phys. **10**, 3454 (2008).
[29] I. Tamm, J. Phys. (USSR) **9**, 449 (1945).
[30] S. M. Dancoff, Phys. Rev. **78**, 382 (1950).
[31] D. Bohm and D. Pines, Phys. Rev. **92**, 609 (1953).
[32] E. R. Davidson, J. Comput. Phys. **17**, 87 (1975).
[33] J. Olsen, H. J. A. Jensen, and P. Jørgensen, J. Comput. Phys. **74**, 265 (1988).
[34] A. Bijl, J. de Boer, and A. Michels, Physica (Amsterdam) **8**, 655 (1941).
[35] R. P. Feynman, Phys. Rev. **94**, 262 (1954).
[36] A. Auerbach, *Interacting Electrons and Quantum Magnetism* (Springer, 1998).
[37] J. Haegeman, S. Michalaks, B. Nachtergaele, T. J. Osborne, N. Schuch, and F. Verstraete, Phys. Rev. Lett. **111**, 080401 (2013).
[38] P. Tavan and K. Schulten, Phys. Rev. B **36**, 4337 (1987).
[39] I. Ohmine, M. Karplus, and K. Schulten, J. Chem. Phys. **68**, 2298 (1978).
[40] D. Ghosh, J. Hachmann, T. Yanai, and G. K.-L. Chan, J. Chem. Phys. **128**, 144117 (2008).